



#1 JOURNAL IN 2014 GOOGLE SCHOLAR METRICS  
FOR THE PLASMA & FUSION CATEGORY

## Coulomb crystal mixtures in white dwarf cores and neutron star crusts

A. A. Kozhberov and D. A. Baiko

Citation: *Physics of Plasmas* **22**, 092903 (2015); doi: 10.1063/1.4930215

View online: <http://dx.doi.org/10.1063/1.4930215>

View Table of Contents: <http://scitation.aip.org/content/aip/journal/pop/22/9?ver=pdfcov>

Published by the AIP Publishing

---

### Articles you may be interested in

The accretion of solar material onto white dwarfs: No mixing with core material implies that the mass of the white dwarf is increasing

AIP Advances **4**, 041007 (2014); 10.1063/1.4866984

#### Polarized pairing in neutron star crusts

AIP Conf. Proc. **1441**, 390 (2012); 10.1063/1.3700564

#### The Electrodynamics of the Core and the Crust components in Neutron Stars

AIP Conf. Proc. **1059**, 68 (2008); 10.1063/1.3012286

#### Magnetic fields in neutron stars, white dwarfs and implications for binary millisecond pulsars

AIP Conf. Proc. **968**, 188 (2008); 10.1063/1.2840393

#### Multi-Dimensional Simulations of the Accretion-Induced Collapse of White Dwarfs to Neutron Stars

AIP Conf. Proc. **924**, 126 (2007); 10.1063/1.2774849

---



**PFEIFFER VACUUM**

**VACUUM SOLUTIONS  
FROM A SINGLE SOURCE**

Pfeiffer Vacuum stands for innovative and custom vacuum solutions worldwide, technological perfection, competent advice and reliable service.



# Coulomb crystal mixtures in white dwarf cores and neutron star crusts

A. A. Kozhberov<sup>a)</sup> and D. A. Baiko  
Ioffe Institute, Politekhnicheskaya 26, St. Petersburg, Russia

(Received 2 July 2015; accepted 20 August 2015; published online 17 September 2015)

We calculate electrostatic, spectral, and thermal properties of two-component Coulomb crystals of ions and determine the limits of applicability of the linear mixing theory to such systems. © 2015 AIP Publishing LLC. [<http://dx.doi.org/10.1063/1.4930215>]

## I. INTRODUCTION

It is generally accepted that matter in white dwarf cores and neutron star envelopes at not too low densities represents a mixture of atomic nuclei of various types immersed into a strongly degenerate electron gas and fully ionized by the gas pressure (e.g., Ref. 1). In particular, the inner layers of white dwarfs are composed of a carbon and oxygen plasma with traces of other elements such as neon and iron (e.g., Ref. 2). At the initial stages of evolution, this mixture is in a liquid state (a Coulomb liquid of ions). As a star cools, the plasma crystallizes with a formation of a Coulomb crystal of ions. The occurrence of this crystallization process has been inferred from observations of a white dwarf in the globular cluster NGC 6397.<sup>3</sup>

In plasma physics, a Coulomb crystal is a system of point charges of one sign arranged in a crystal lattice with a strictly uniform neutralizing background of opposite charge (e.g., Refs. 1 and 4). It is customary to consider Coulomb crystals with a single ion type (one-component crystals or occ). If quantization of the ion motion is neglected, the properties of this system are determined by one parameter, the Coulomb coupling parameter  $\Gamma \equiv (Z_i e)^2 / (a_i T)$ . In this case,  $Z_i e$  is the ion charge,  $T$  is the temperature ( $k_B = 1$ ),  $a_i = (4\pi n_i/3)^{-1/3}$  is the ion sphere radius, and  $n_i$  is the ion number density. Such classic occ is known to melt at  $\Gamma \approx 175$  (e.g., Ref. 1).

In the compact stars, one typically expects  $\Gamma \gg 1$ . Moreover, in the crusts of neutron stars,  $\Gamma > 175$  except the outermost low-density layers and/or the very early stages of the star life. Therefore, for astrophysical applications, it is necessary to study thermodynamic properties of Coulomb crystals (both occ and mixtures). For instance, heat capacity of matter in the inner layers of white dwarfs controls the cooling rate and is thus required for a reliable estimate of the star age (e.g., Refs. 2 and 4). Precise knowledge of the electrostatic energy and thermal free energy is indispensable for determination of the crystallization temperature.

Thermodynamic properties of occ in the harmonic lattice approximation have been studied in Refs. 5–7 and fitted with comparable accuracy for body-centered cubic (bcc) and face-centered cubic (fcc) lattices in Refs. 8 and 9. The influence of magnetic field on thermodynamics of occ was analyzed in detail in Refs. 10 and 11, while electron

screening has been discussed in Refs. 12–14. Various analytic and numerical methods were employed to study classic and quantum anharmonic corrections in a large number of works (e.g., Refs. 9, 15, 16, and references therein). Among all investigated lattices the bcc lattice was found to have the lowest free energy, but the difference between the energies of several lattices is very small, and, if the electron polarization is taken into account, the fcc lattice may become more energetically favorable.<sup>13</sup>

Far less work has been devoted to a description of Coulomb mixtures, i.e., multi-component plasmas composed of fully ionized atomic nuclei of several types and a uniform charge-compensating electron background (e.g., Ref. 17). Physical properties of these systems are usually obtained from the linear mixing (lm) theory (e.g., Refs. 18 and 19) or numerically, from molecular dynamics (e.g., Refs. 20–22 and references therein) or Monte-Carlo (e.g., Refs. 23–26) simulations. A high level of accuracy of the lm approach for the Coulomb liquid has been demonstrated<sup>27</sup> and confirmed later by Monte-Carlo modeling (e.g., Refs. 25 and 28). The lm rule has been applied to Coulomb crystals for the first time in Ref. 29. These authors calculated the electrostatic energy of substitutionally disordered (i.e., ions of different types are randomly distributed over nodes of a perfect lattice) bcc, fcc, and CsCl lattices as an average of the local minima of the interaction energies, obtained from several independent molecular dynamics runs, and made a comparison with respective lm predictions. Recently, a simple analytic estimate of the free energy deviation from the lm result has been proposed.<sup>19</sup>

Unfortunately, none of these methods is applicable at temperatures below the crystal Debye temperature, where quantum effects of the ion motion play a decisive role, and thus, there is no assessment of the validity of the lm theory under such conditions. However, the quantum regime is highly relevant for the astrophysical objects mentioned above.

In this paper, we refine and expand our work<sup>30</sup> and present a detailed analytic and numerical study of physical properties of an ordered binary Coulomb crystal, i.e., a perfect Coulomb crystal with ions of two different sorts (different charges and masses) in each elementary cell. We focus on thermodynamic functions of the ion component only treating electrons simply as a uniform neutralizing background. In principle, thermodynamic functions of strongly degenerate electron gas are well understood and should be added

<sup>a)</sup>Electronic mail: kozhberov.astro@mail.ioffe.ru.

directly to the respective ion contributions. Let us note that electrons are responsible for the dominant contribution to the crystal pressure and for a substantial contribution to the system heat capacity, particularly at low temperatures. We analyze electrostatic, spectral, and thermal properties of the binary Coulomb crystal mixture within the harmonic lattice model framework. This allows us to take into account the quantum effects. For simplicity, we neglect anharmonic effects, which become significant near the melting transition, as well as effects of the electron background polarization. The latter invalidate the assumption of constant and uniform electron background and are important for large-Z ions at rather low densities. We compare our results with predictions of the lm theory and discuss its applicability to Coulomb crystal mixtures at low temperatures.

## II. NOTATIONS

Consider an ordered Coulomb crystal mixture (or a multi-component Coulomb crystal), i.e., a regular arrangement of ions of several types in a lattice. The position of an ion of type  $p$  (with charge number  $Z_p$  and mass  $M_p$ ,  $p = 1 \dots N_{\text{cell}}$ ,  $N_{\text{cell}}$  is the number of ions in the lattice elementary cell) in a crystal is given by its radius vector  $\mathbf{r}_{lp} = \mathbf{X}_{lp} + \mathbf{u}_{lp}$ , where  $\mathbf{u}_{lp}$  is the ion displacement from its equilibrium position. Equilibrium positions of ions are given by  $\mathbf{X}_{lp} = \mathbf{R}_l + \chi_p$ , where  $\mathbf{R}_l = l_1 \mathbf{a}_1 + l_2 \mathbf{a}_2 + l_3 \mathbf{a}_3$  is a lattice vector,  $l_1, l_2, l_3$  are arbitrary integers, vectors  $\mathbf{a}_1, \mathbf{a}_2, \mathbf{a}_3$  are the lattice main translation vectors, and  $\chi_p$  is the basis vector of the  $p$ -ion in the elementary cell (by construction we always have  $\chi_1 = 0$ ,  $\chi_p \neq 0$  for  $p > 1$ ). The reciprocal lattice is formed by vectors  $\mathbf{G}_m = m_1 \mathbf{g}_1 + m_2 \mathbf{g}_2 + m_3 \mathbf{g}_3$ , where  $\mathbf{g}_1, \mathbf{g}_2, \mathbf{g}_3$  are the reciprocal lattice main translation vectors satisfying  $\mathbf{g}_i \cdot \mathbf{a}_j = 2\pi \delta_{ij}$ , and  $m_1, m_2, m_3$  are arbitrary integers.

We shall study in detail and compare two binary lattices: a simple cubic lattice with  $N_{\text{cell}} = 2$  (sc2) and a hexagonal lattice with  $N_{\text{cell}} = 2$  (h2). The ions at  $\chi_1$  and  $\chi_2$  are different, while the number density is the same for ions of both types. Figure 1 illustrates the two lattice structures with different colors corresponding to different ions. The sc2 and h2 lattices coincide with the bcc and hexagonal close-packed (hcp) lattices, respectively, if all ions are identical. The origin of a Cartesian coordinate system is always assumed to coincide with a  $Z_1$ -ion, while  $\alpha \equiv Z_2/Z_1 \geq 1$ . We shall describe the sc2 lattice by the simple cubic (sc) lattice main translation

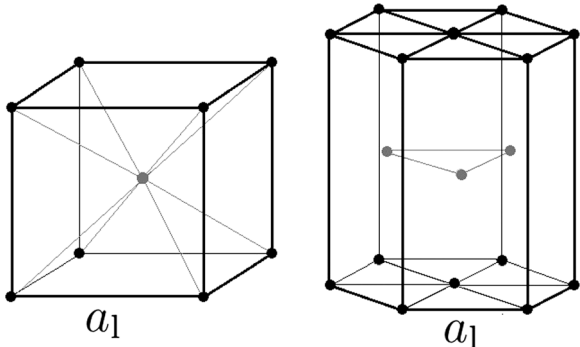


FIG. 1. The sc2 (left) and h2 (right) lattices.

vectors  $\mathbf{a}_1 = a_1(1, 0, 0)$ ,  $\mathbf{a}_2 = a_1(0, 1, 0)$ ,  $\mathbf{a}_3 = a_1(0, 0, 1)$ , and the basis vector  $\chi_2 = 0.5a_1(1, 1, 1)$ . The h2 lattice is described by the main translation vectors of the hexagonal (hex) lattice  $\mathbf{a}_1 = a_1(1, 0, 0)$ ,  $\mathbf{a}_2 = 0.5a_1(1, \sqrt{3}, 0)$ , and  $\mathbf{a}_3 = a_1(0, 0, \sqrt{8/3})$  with the basis vector  $\chi_2 = a_1(1/3, 1/3, \sqrt{2/3})$ . In both cases,  $a_1$  is the lattice constant (cf. Fig. 1). The primitive subzones of the Brillouin zones of these lattices are determined by the following inequalities:  $k_x \geq k_y \geq k_z \geq 0$ ,  $k_x a_1 \leq \pi$  for the sc2 lattice, and  $0 \leq k_x a_1 \leq \pi \sqrt{4/3}$ ,  $0 \leq k_y \leq k_x / \sqrt{3}$ , and  $0 \leq k_z a_1 \leq \pi \sqrt{3/8}$  for the h2 lattice, where  $\mathbf{k}$  is a wavevector.

## III. ELECTROSTATIC ENERGY

The potential energy of a multi-component Coulomb crystal with an arbitrary number and type of ions in the elementary cell is given by

$$U = \frac{1}{2} \sum'_{lp'lp} \frac{Z_p Z_{p'} e^2}{|\mathbf{r}_{lp} - \mathbf{r}_{l'p'}|} - n_e \sum_{lp} \int d\mathbf{r} \frac{Z_p e^2}{|\mathbf{r}_{lp} - \mathbf{r}|} + \frac{n_e^2 e^2}{2} \iint \frac{d\mathbf{r} d\mathbf{r}'}{|\mathbf{r} - \mathbf{r}'|}, \quad (1)$$

where sums over  $l$  and  $l'$  are extended to infinity, sums over  $p$  and  $p'$  go over all ions in the elementary cell, prime at the first sum means that terms with  $l = l'$  and  $p = p'$  are omitted,  $Z_p$  is the charge number of ions located at  $\mathbf{r}_{lp}$ ,  $n_e = Zn$  is the electron number density,  $Z$  is the average ion charge number, and  $n$  is the total ion number density. For binary crystals considered in this work,  $n_e = 0.5n(Z_1 + Z_2)$ . The first sum is divergent, whereas the second and the third terms serve to cancel this infinity, so that the electrostatic energy per one ion becomes finite.

If all ions are fixed at their equilibrium positions,  $\mathbf{r}_{lp} = \mathbf{X}_{lp}$ , Eq. (1) yields the static-lattice binding energy of the crystal, or the Madelung energy,  $U_M$ . Equation (1) is obviously impractical and we have used Ewald transformations<sup>31</sup> to derive a rapidly converging practical formula for calculating the Madelung energy of a completely general perfectly ordered multi-component Coulomb crystal

$$U_M = N \frac{e^2}{a} \xi, \quad \xi = \frac{a}{2N_{\text{cell}}} \sum_{lp'p} Z_p Z_{p'} (1 - \delta_{pp'} \delta_{R_l 0}) \frac{\text{erfc}(AY_{lp'})}{Y_{lp'}} - \frac{Aa}{N_{\text{cell}} \sqrt{\pi}} \sum_p Z_p^2 - \frac{3}{8N_{\text{cell}}^2 A^2 a^2} \sum_{pp'} Z_p Z_{p'} + \frac{3}{2N_{\text{cell}}^2 a^2} \sum_{mpp'} Z_p Z_{p'} (1 - \delta_{G_m 0}) \times \frac{1}{G_m^2} \exp \left[ -\frac{G_m^2}{4A^2} + i \mathbf{G}_m (\chi_p - \chi_{p'}) \right]. \quad (2)$$

In this case,  $\mathbf{Y}_{lp'} = \mathbf{R}_l + \chi_p - \chi_{p'}$ ,  $N$  is the total number of ions,  $a \equiv (4\pi n/3)^{-1/3}$ , and  $\text{erfc}(x)$  is the complementary error function. An arbitrary parameter  $A$  is chosen so that sums over direct and reciprocal lattice vectors,  $\mathbf{R}_l$  and  $\mathbf{G}_m$ ,

converge equally rapidly. Equation (2) reproduces Eq. (10) of Ref. 32 for an occ with  $N_{\text{cell}} = 1$ . For an occ with  $N_{\text{cell}} > 1$ , this formula reproduces, e.g., Eq. (5) of Ref. 8. For multi-component crystals, to our knowledge, such a formula has not been previously published.

For ordered binary crystal mixtures in consideration, Eq. (2) reduces to<sup>30</sup>

$$U_M = N \frac{e^2}{a} \left[ \frac{Z_1^2 + Z_2^2}{2^{4/3}} \zeta_1 + Z_1 Z_2 \left( \zeta_2 - \frac{\zeta_1}{2^{1/3}} \right) \right]. \quad (3)$$

In the case of the sc2 lattice,  $\zeta_1$  and  $\zeta_2$  are the Madelung constants of the sc and bcc lattices, respectively ( $\zeta_1 = \zeta_{\text{sc}} = -0.88005944211$  and  $\zeta_2 = \zeta_{\text{bcc}} = -0.89592925568$ ). For the h2 lattice,  $\zeta_1$  and  $\zeta_2$  are the Madelung constants of the hex and hcp lattices, respectively ( $\zeta_1 = \zeta_{\text{hex}} = -0.77943336427$  and  $\zeta_2 = \zeta_{\text{hcp}} = -0.89583812046$ ). It is clear, that in the special cases  $Z_1 = Z_2$  and  $Z_2 = 0$ , Eq. (3) reproduces correctly the Madelung energy of the respective occ.

Interestingly, Eq. (3) can be easily obtained from symmetry considerations. Since densities of both types of ions are equal and the lattices do not change under the ion interchange ( $Z_1 \leftrightarrow Z_2$ ), the electrostatic energy must have the form:  $U_M = c_1(Z_1^2 + Z_2^2) + c_2 Z_1 Z_2$ . Constants  $c_1$  and  $c_2$  can now be found from the special cases above. If  $Z_2 = 0$ , the number of ions is halved and  $c_1 = Ne^2 \zeta_1 / (2^{4/3} a)$ . If  $Z_1 = Z_2$ ,  $2c_1 + c_2 = Ne^2 \zeta_2 / a$ .

It is useful to compare the exact Madelung energy with that obtained from the lm theory. According to Ref. 18, linear mixing yields the Madelung energy of a binary crystal as

$$U_M^{\text{lm}} = N_1 \frac{Z_1^2 e^2}{a_1} \zeta_2 + N_2 \frac{Z_2^2 e^2}{a_2} \zeta_2, \quad (4)$$

where  $a_j = (4\pi n_j/3)^{-1/3}$ ,  $n_j = n_e/Z_j$ , and the electron number density  $n_e$  in both terms should be the same as in the mixture;  $N_j$  is the total number of  $j$ -ions. Hence, for a perfectly ordered binary crystal with  $N_1 = N_2$ ,

$$\frac{U_M^{\text{lm}}}{U_M} = \frac{(1+\alpha)^{1/3}(1+\alpha^{5/3})\zeta_2}{(\alpha-1)^2\zeta_1+2^{4/3}\alpha\zeta_2}. \quad (5)$$

---


$$B_{pp'}^{\mu\lambda}(\mathbf{k}) = \frac{4\pi n}{N_{\text{cell}}} \sum_m \frac{(G_m^\mu - k^\mu)(G_m^\lambda - k^\lambda)}{|\mathbf{G}_m - \mathbf{k}|^2} \exp \left[ -\frac{|\mathbf{G}_m - \mathbf{k}|^2}{4A^2} + i(\mathbf{G}_m - \mathbf{k})(\chi_p - \chi_{p'}) \right] - \frac{4A^3}{3\sqrt{\pi}} \delta^{\mu\lambda} \delta_{pp'} \\ - \sum_l (1 - \delta_{pp'} \delta_{Rl0}) \left\{ \left( \frac{3Y_{lpp'}^\alpha Y_{lpp'}^\lambda}{Y_{lpp'}^2} - \delta^{\mu\lambda} \right) \left[ \frac{\text{erfc}(AY_{lpp'})}{Y_{lpp'}^3} + \frac{2A}{\sqrt{\pi}Y_{lpp'}^2} e^{-A^2 Y_{lpp'}^2} \right] + \frac{4A^3}{\sqrt{\pi}} \frac{Y_{lpp'}^\mu Y_{lpp'}^\lambda}{Y_{lpp'}^2} e^{-A^2 Y_{lpp'}^2} \right\} e^{i\mathbf{k}\mathbf{R}_l}, \\ W_p^{\mu\lambda} = -\frac{4\pi n}{N_{\text{cell}}} \sum_{p''} Z_{p''} \sum_m' \frac{G_m^\mu G_m^\lambda}{G_m^2} \exp \left[ -\frac{G_m^2}{4A^2} + i\mathbf{G}_m(\chi_p - \chi_{p''}) \right] + \frac{4A^3}{3\sqrt{\pi}} Z_p \delta^{\mu\lambda} \\ + \sum_{lp''} Z_{p''} (1 - \delta_{pp''} \delta_{Rl0}) \left\{ \left( \frac{3Y_{lpp''}^\mu Y_{lpp''}^\lambda}{Y_{lpp''}^2} - \delta^{\mu\lambda} \right) \left[ \frac{\text{erfc}(AY_{lpp''})}{Y_{lpp''}^3} + \frac{2A}{\sqrt{\pi}Y_{lpp''}^2} e^{-A^2 Y_{lpp''}^2} \right] + \frac{4A^3}{\sqrt{\pi}} \frac{Y_{lpp''}^\mu Y_{lpp''}^\lambda}{Y_{lpp''}^2} e^{-A^2 Y_{lpp''}^2} \right\}, \quad (8)$$

Equation (5) is symmetric under the replacement of  $\alpha$  by  $1/\alpha$ , is 1 at  $\alpha = 1$ , and reaches 1.00094 and 1.00215 for the sc2 and h2 lattices, respectively, at the maximum allowed charge ratio for these lattices,  $\alpha = 3.6$  and  $\alpha = 1.25$  (see below). For the carbon-oxygen mixture with the sc2 lattice,  $U_M^{\text{lm}}/U_M - 1 \approx -6.67 \times 10^{-5}$ . This difference seems small, but it may still be important, because the Madelung energy is by far the dominant contribution to the crystal energy. For some applications (such as determination of the crystal melting point), it is desirable to know it with the best possible precision.

#### IV. DYNAMIC MATRIX AND COLLECTIVE MODES

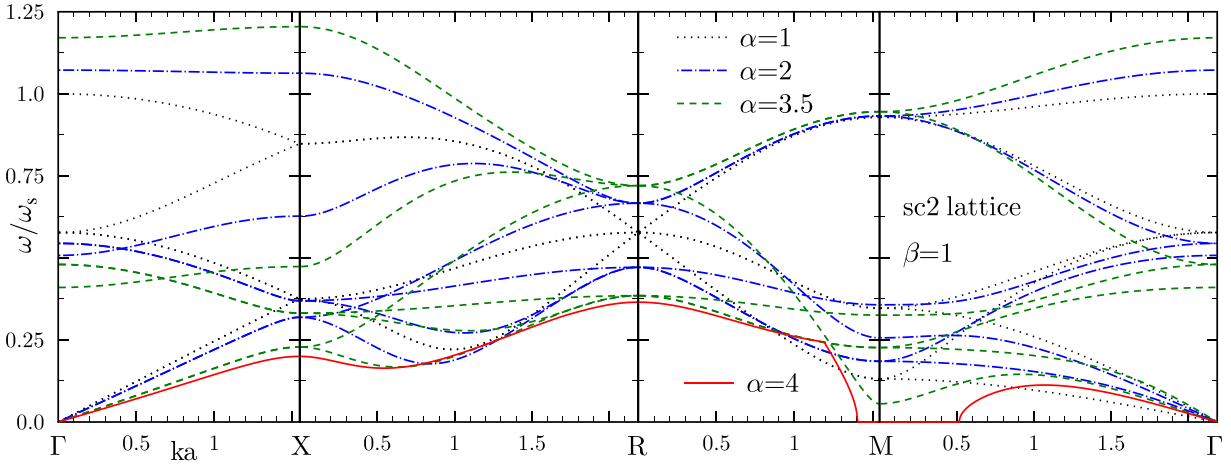
The potential energy Eq. (1) can be expanded in powers of ion displacements and, in the harmonic lattice model, only the second order terms are retained. These terms determine the phonon spectrum of the crystal, which can be found by solving the dispersion equation  $\det\{D_{pp'}^{\mu\lambda}(\mathbf{k}) - \omega^2 \delta^{\mu\lambda} \delta_{pp'}\} = 0$  for the squared frequency,  $\omega^2$ , at any wavevector  $\mathbf{k}$ . For a perfect lattice with arbitrary number and type of ions in the elementary cell, the dynamic matrix  $D_{pp'}^{\mu\lambda}(\mathbf{k})$  is equal to

$$D_{pp'}^{\mu\lambda}(\mathbf{k}) = \frac{Z_p Z_{p'} e^2}{\sqrt{M_p M_{p'}}} B_{pp'}^{\mu\lambda}(\mathbf{k}) + \frac{Z_p e^2}{M_p} W_p^{\mu\lambda} \delta_{pp'}, \quad (6)$$

where

$$B_{pp'}^{\mu\lambda}(\mathbf{k}) = -\frac{\partial^2}{\partial u^\mu \partial u^\lambda} \sum_{\mathbf{R}_l \neq 0} \frac{\exp(i\mathbf{k}\mathbf{R}_l)}{|\mathbf{u} - \mathbf{R}_l - \chi_p + \chi_{p'}|} \Big|_{\mathbf{u} \rightarrow 0}, \\ W_p^{\mu\lambda} = \frac{\partial^2}{\partial u^\mu \partial u^\lambda} \left\{ \sum_{\mathbf{R}_l \neq 0} \sum_{p''} \frac{Z_{p''}}{|\mathbf{u} - \mathbf{R}_l - \chi_p + \chi_{p''}|} \right. \\ \left. - n_e \int \frac{d\mathbf{r}}{|\mathbf{u} - \chi_p - \mathbf{r}|} \right\} \Big|_{\mathbf{u} \rightarrow 0}. \quad (7)$$

Using Ewald transformations one can recast matrices  $B_{pp'}^{\mu\lambda}(\mathbf{k})$  and  $W_p^{\mu\lambda}$  in a form of rapidly converging lattice sums,<sup>30</sup> which we reproduce here for completeness

FIG. 2. Phonon frequencies of the sc2 lattice in certain high-symmetry directions for  $\beta=1$  and several values of  $\alpha$ .

where  $\mathbf{Y}_{lpp''} = \mathbf{R}_l + \chi_p - \chi_{p''}$ , indices  $\mu, \lambda$  denote Cartesian components, and  $A$  is again arbitrary. For cubic occ with  $N_{\text{cell}} = 1$ , Eqs. (6) and (8) reproduce Eq. (3) of Ref. 8. For non-cubic occ (e.g., for hcp), Eq. (3) of Ref. 8 is incorrect.

One can show<sup>30</sup> that

$$\sum_{\nu} \omega_{\nu}^2(\mathbf{k}) = N_{\text{cell}} \omega_s^2, \quad (9)$$

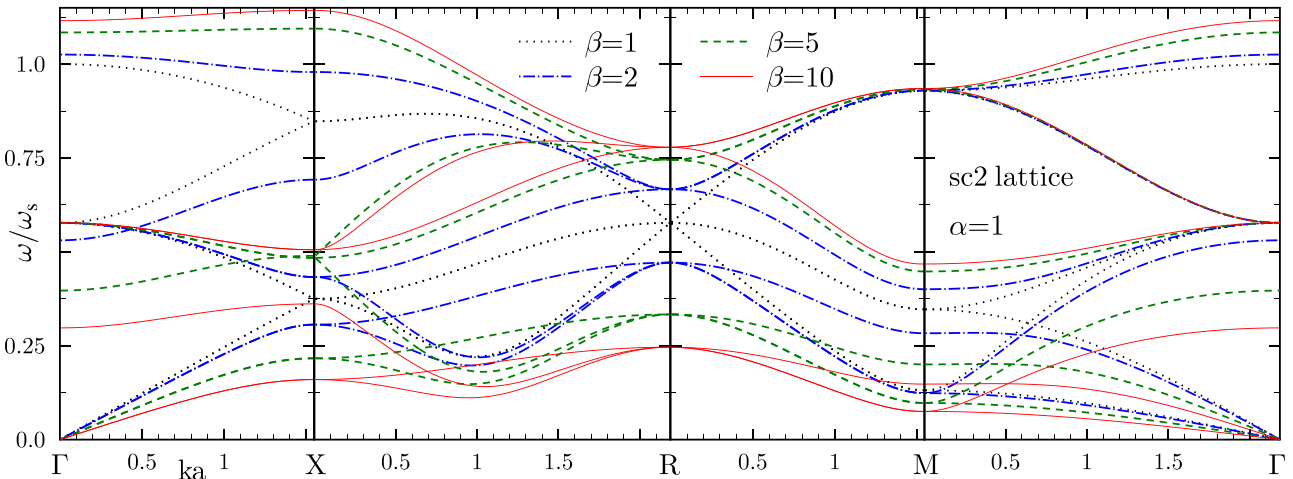
$$\omega_s^2 = \frac{4\pi n e^2}{N_{\text{cell}}^2} \sum_{pp'} \frac{Z_p Z_{p'}}{M_p}, \quad (10)$$

where  $\nu$  enumerates frequencies at fixed  $\mathbf{k}$  ( $\nu = 1 \dots 3N_{\text{cell}}$ ). For an occ with  $N_{\text{cell}} \geq 1$ ,  $Z_p = Z$ , and  $M_p = M$  for all  $p$ ,  $\omega_s$  becomes the regular plasma frequency  $\omega_p = \sqrt{4\pi n Z^2 e^2 / M}$ . For this reason,  $\omega_s$  can be called the multi-component plasma frequency. An occ can also be obtained by setting  $Z_p$  to  $Z$  and  $M_p$  to  $M$  for some values of  $p$ , and  $Z_p = 0$  for all the other values of  $p$ . Equation (9) will yield a correct sum rule in this case as well.

For binary crystals under consideration,  $\omega_s = [\pi n Z_1^2 e^2 (1 + \alpha)(1 + \alpha/\beta)/M_1]^{1/2}$  and the spectrum depends on wave-vector  $\mathbf{k}$  and two parameters,  $\alpha = Z_2/Z_1$  and  $\beta \equiv M_2/M_1$ . In Figs. 2–5, we plot dispersion curves of the sc2 and h2 lattices

in several high-symmetry directions for various  $\alpha$  and  $\beta$  as functions of the distance from the respective Brillouin zone vertex measured in units of  $1/a$ . Also, we plot dispersion curves of the bcc and hcp lattices (case  $\alpha = \beta = 1$ ), which coincide with those shown in Refs. 33 and 34, respectively. We use standard notations for the vertices of the primitive subzones of the Brillouin zones of the sc and hex lattices (e.g., Ref. 35). For instance,  $\Gamma$  denotes the first Brillouin zone center. At any  $\mathbf{k}$ ,  $\alpha$ , and  $\beta$ , the phonon spectrum consists of six modes. Two of them are acoustic ( $\omega \propto k$  at small  $k$ ) and the others are optic ( $\omega$  is finite at  $k=0$ ).

In a stable Coulomb crystal in the harmonic lattice approximation, the phonon frequencies cannot acquire imaginary parts. By this criterion, the sc2 lattice can exist only up to  $\alpha = 3.60$  (by definition  $\alpha \geq 1$ ), whereas the h2 lattice is stable only up to  $\alpha = 1.25$ .<sup>30</sup> (The same result for the sc2 lattice was recently found in molecular dynamics simulations.<sup>38</sup>) Hence, for instance, the one-to-one  $^{12}\text{C} + ^{16}\text{O}$  mixture cannot crystallize into the perfect h2 lattice. These results are not surprising given the fact that the bcc and hcp lattices are stable while the sc and hex lattices (which can be viewed as the sc2 and h2 lattices with  $\alpha = \infty$ ) are not.<sup>36,37</sup> For illustration, in Fig. 2, we plot the lowest frequency of the sc2 lattice at  $\alpha = 4$ . Its real part becomes 0 near the point M,

FIG. 3. Same as in Fig. 2 but for  $\alpha=1$  and several values of  $\beta$ .

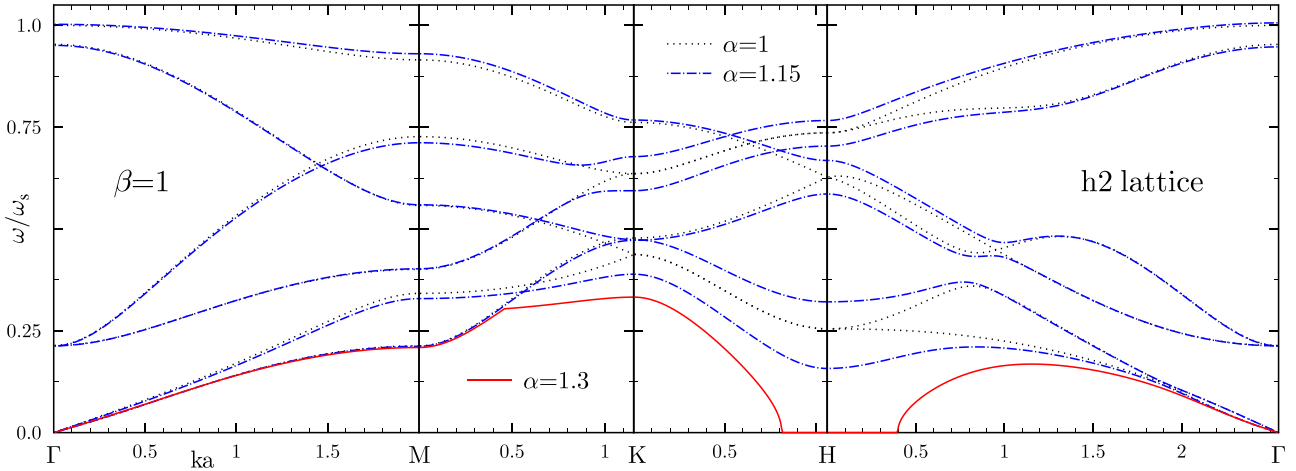


FIG. 4. Same as in Fig. 2 but for the h2 lattice.

and the frequency becomes imaginary. The same picture can be observed in Fig. 4 for the h2 lattice with  $\alpha = 1.3$ .

Ion masses do not affect the crystal stability. For completeness, we have investigated the properties of lattice phonons in the limit of very different ion masses ( $M_2 \gg M_1$  or  $M_2 \ll M_1$ ) at similar ion charges. (This limit may be relevant for compact star matter at lower densities, where there is partial ionization and the concept of effective ion charge is thought to be adequate.) In this regime, there appear two widely separated groups of phonon modes (Fig. 6). The three upper modes describe the oscillations of the lighter ions with respect to the heavier ones. The frequencies of these oscillations, normalized by  $\omega_s$ , do not depend on  $\beta$ . The three lower modes describe the joint motion of all ions, in which the kinetic energy of the lighter ones is negligible. For these modes,  $\omega_\nu(\mathbf{k})/\omega_s$  scales as  $\beta^{-0.5}$  at  $\beta \gg 1$  ( $\omega_\nu(\mathbf{k})/\omega_s \propto \beta^{0.5}$  at  $\beta \ll 1$ ), while the shape of the modes essentially does not change.

## V. FREQUENCY SPECTRUM MOMENTS AND THE ENERGY OF ZERO-POINT VIBRATIONS

In applications, it is often necessary to know averages of various functions of phonon frequencies over the phonon phase space. Such an average can be written as

$$\langle f(\omega) \rangle = \frac{1}{3N_{\text{cell}}} \sum_{\nu} \frac{1}{V_{\text{BZ}}} \int_{\text{BZ}} f(\omega_{\nu}(\mathbf{k})) d\mathbf{k}, \quad (11)$$

where the integration is over the whole volume of the first Brillouin zone  $V_{\text{BZ}} = (2\pi)^3 n / N_{\text{cell}}$  and the summation at each  $\mathbf{k}$  runs over all  $\nu$ . We will use the three-dimensional modified Gaussian quadrature and Holas integration method for such averages.<sup>8,39,40</sup>

Among the most frequently used averages are the moments of the phonon spectrum  $u_n = \langle (\omega/\omega_s)^n \rangle$  and the average logarithm of frequency  $u_{\ln} = \langle \ln(\omega/\omega_s) \rangle$ . The moment  $u_1$  determines the zero-point energy of the crystal, moments  $u_{-1}$  and  $u_{-2}$  yield the rms ion displacement from a lattice node at quantum and classic temperatures, respectively, whereas  $u_{\ln}$  enters the classic asymptote of the Helmholtz free energy.

In a Coulomb occ, the moments in question depend only on the crystal type. But in a binary Coulomb crystal, they also depend on  $\alpha$  and  $\beta$ , which we denote as  $u_i(\alpha, \beta)$ , where  $i$  stands for  $-2, -1, 1$ , or  $\ln$ . The results of our calculations are reported in Figs. 7–9. (For any other parameter values, the data are available upon request.) In Fig. 7, we plot  $u_i(\alpha, \beta) / u_i(\alpha, 1)$  as functions of  $\beta$  at  $\alpha = 1, 2$ , and  $3$  for the sc2 lattice. To avoid numerous intersections of the curves, at

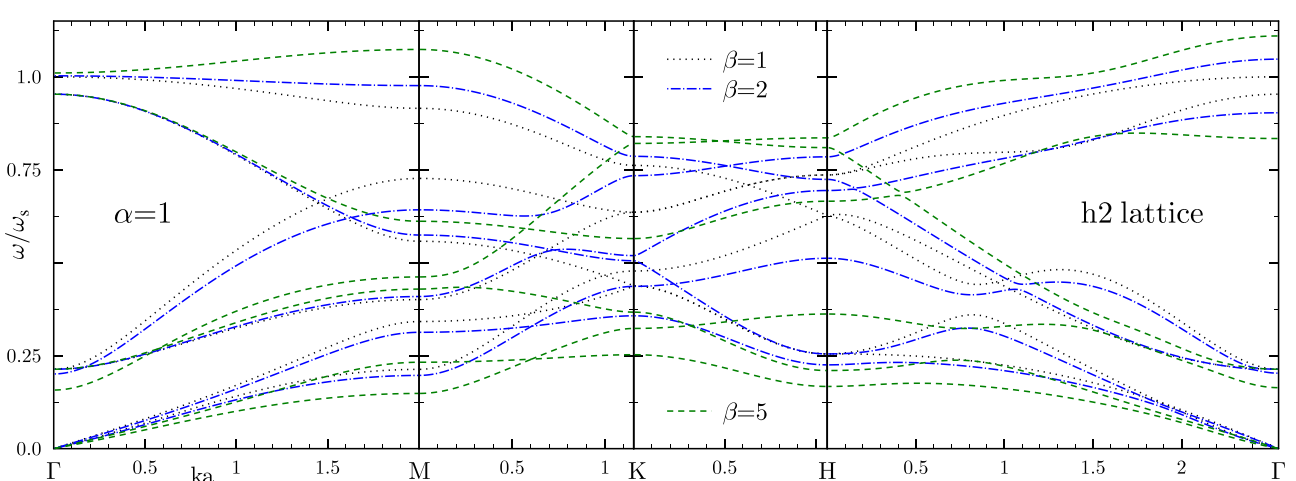


FIG. 5. Same as in Fig. 3 but for the h2 lattice.

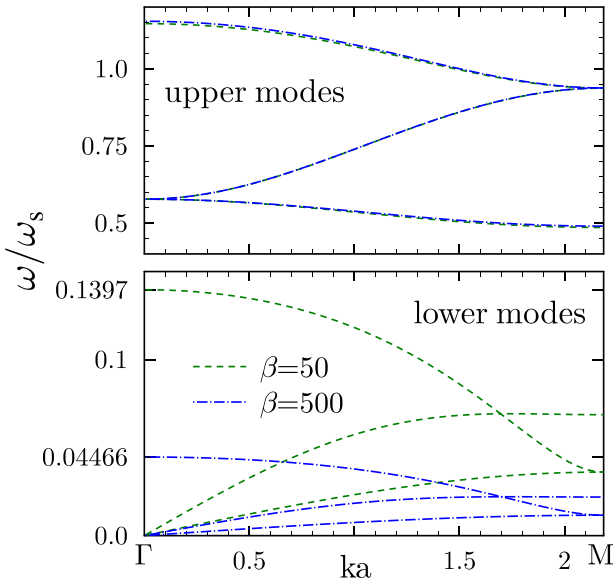
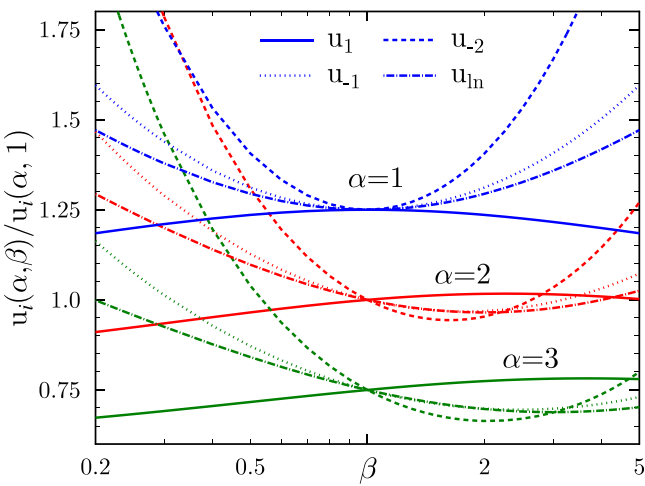
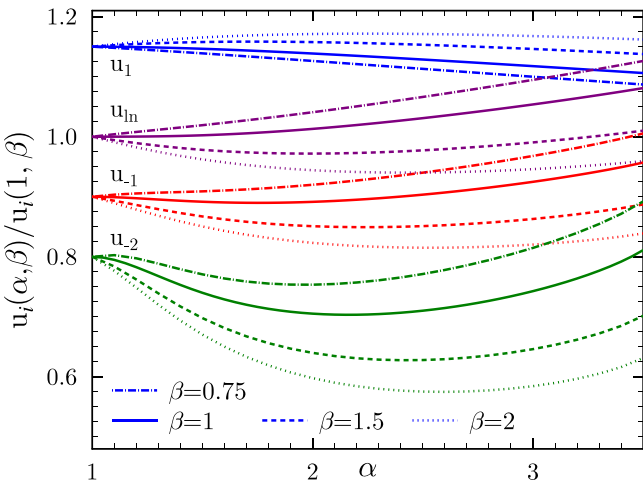
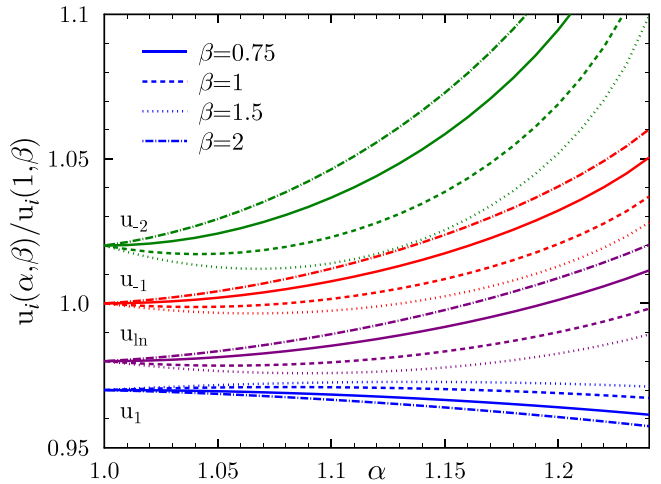
FIG. 6. Dispersion curves for the sc2 lattice at  $M_2 \gg M_1$  and  $\alpha = 1$ .FIG. 7. The dependence of moments on  $\beta$  for  $\alpha = 1, 2$  and  $3$  for the sc2 lattice.FIG. 8. The dependence of moments on  $\alpha$  for different  $\beta$  for the sc2 lattice.

FIG. 9. Same as in Fig. 8 but for the h2 lattice.

$\alpha = 1$  and  $3$ , the ratios are multiplied by  $1.25$  and  $0.75$ , respectively. At  $\alpha = 1$ , the curves for the h2 lattice practically merge with the corresponding curves for the sc2 lattice for this range of  $\beta$  (cf. Fig. 10). Figs. 8 and 9 demonstrate the dependence of the moments on  $\alpha$  for the sc2 and h2 lattices, respectively. In Fig. 8, we show  $u_i(\alpha, \beta)/u_i(1, \beta)$  at  $\beta = 0.75, 1, 1.5$ , and  $2$ . For clarity, in the case of  $u_1$ ,  $u_{-1}$ , and  $u_{-2}$ , the ratios are again multiplied by  $1.15, 0.9$ , and  $0.8$ , respectively. In Fig. 9, everything is the same, but the  $u_{-2}$ ,  $u_{\ln}$ , and  $u_1$  data are multiplied by  $1.02, 0.98$ , and  $0.97$ , respectively, and the range of  $\alpha$ , where the lattice is stable, is much more narrow. The moment values used in the denominators of all these ratios are collected in Table I.

The energy of zero-point vibrations is  $E_0 = 1.5N\hbar\langle\omega\rangle = 1.5N\hbar\omega_s u_1(\alpha, \beta)$ . For the bcc and hcp lattices,  $u_1$  is equal to  $0.51139$  and  $0.51334$ , respectively, and therefore, as is well known, the bcc lattice remains energetically preferred at temperature  $T = 0$  to the hcp lattice, if both electrostatic and zero-point energies are taken into account. However, in a binary crystal with  $\alpha = 1$ ,  $E_0$  for the h2 lattice is bigger than that for the sc2 lattice only at  $1/3.69 \leq \beta \leq 3.69$ .

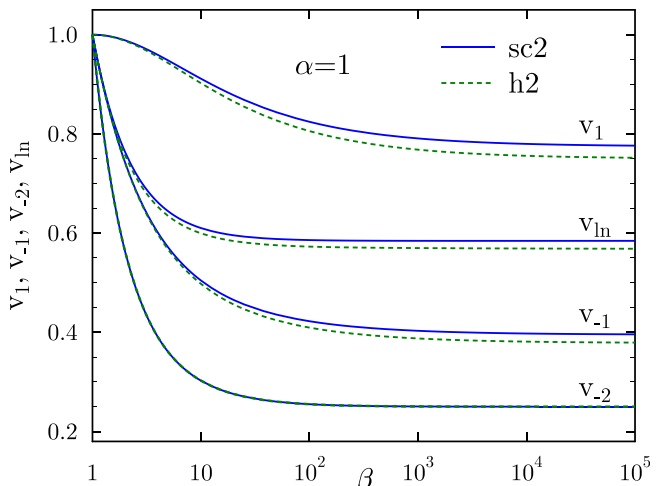
FIG. 10. The behavior of the moments at  $\alpha = 1$  and  $\beta \gg 1$  for the sc2 and h2 lattices. See text for details.

TABLE I. Moments of the sc2 and h2 lattices used to obtain the ratios plotted in Figs. 7–9. The values of  $\alpha$  and  $\beta$  are given in parenthesis.

	sc2 (1,1)	sc2 (1,0.75)	sc2 (1,1.5)	sc2 (1,2)	sc2 (2,1)	sc2 (3,1)	h2 (1,1)	h2 (1,0.75)	h2 (1,1.5)	h2 (1,2)
$u_1$	0.5113877	0.51034	0.509323	0.505521	0.506311	0.496956	0.5133369	0.512183	0.511061	0.506868
$u_{-1}$	2.79853	2.82212	2.84545	2.93644	2.77208	2.87589	2.70183	2.72385	2.74563	2.83054
$u_{-2}$	12.9725	13.2431	13.5131	14.5941	11.4364	12.0446	11.8421	12.0888	12.3356	13.3225
$-u_{\ln}$	0.831295	0.836452	0.841501	0.860741	0.84212	0.875976	0.816031	0.821185	0.826236	0.845477

Accordingly, for systems with a sufficiently large mass ratio the h2 lattice may become energetically preferred at  $T=0$  to the sc2 lattice. On the other hand, at  $\alpha=1.2$ ,  $u_1(1.2, \beta)$  for the sc2 lattice is always bigger than that for the h2 lattice. Hence, for such charge ratio, there are densities at which the h2 lattice is more favorable regardless of the mass ratio.<sup>41</sup>

Let us also discuss the behavior of the spectral averages in the limit of a very large mass ratio of the constituent ions, where some analytic results can be obtained. Clearly, for  $u_1(\alpha, \beta)$ , the three upper frequencies  $\omega \sim \omega_s$  produce the dominant contribution. Thus, at  $\beta \gg 1$  or  $\beta \ll 1$ ,  $u_1(\alpha, \beta)$  approaches a constant value. This can be seen in Fig. 10, where we plot  $v_1 \equiv u_1(1, \beta)/u_1(1, 1)$  as a function of  $\beta$ . The opposite situation takes place for  $u_{-1}(\alpha, \beta)$  and  $u_{-2}(\alpha, \beta)$ . The three lower modes yield the dominant contribution to these moments and, consequently,  $u_{-1}(\alpha, \beta)$  behaves as  $\beta^{0.5}$  at  $\beta \gg 1$  ( $\beta^{-0.5}$  at  $\beta \ll 1$ ), while  $u_{-2}(\alpha, \beta)$  grows  $\propto \beta$  ( $\propto 1/\beta$ ) at  $\beta \gg 1$  ( $\beta \ll 1$ ). In Fig. 10, we show  $v_{-1} \equiv u_{-1}(1, \beta)/u_{-1}(1, 1)/\sqrt{\beta}$  and  $v_{-2} \equiv u_{-2}(1, \beta)/u_{-2}(1, 1)/\beta$ . As expected, these quantities approach constant values at  $\beta \gg 1$ . Finally, in the case of  $u_{\ln}$  both groups of modes produce comparable contributions. The upper modes result in a constant term and the lower modes yield a  $\propto \ln \beta$  term in the high- $\beta$  asymptote. It is illustrated in Fig. 10, where  $v_{\ln} \equiv u_{\ln}(1, \beta)/u_{\ln}(1, 1)/(1 + q_1 \ln \beta)$  is plotted with  $q_1 = 0.5214$  for the sc2 lattice and  $q_1 = 0.5313$  for the h2 lattice. All these conclusions also hold for  $\alpha > 1$ .

## VI. PHONON THERMODYNAMICS

Thermal phonon Helmholtz free energy  $F$ , thermal phonon energy  $U$ , and heat capacity  $C$  are given by

$$\begin{aligned} F &= 3NT\langle \ln(1 - e^{-w}) \rangle, \\ U &= 3NT\left\langle \frac{w}{e^w - 1} \right\rangle, \\ C &= 3N\left\langle \frac{w^2}{4\sinh^2(w/2)} \right\rangle, \end{aligned} \quad (12)$$

where  $w \equiv \hbar\omega/T$  and phonon chemical potential is zero. The thermodynamic potentials of a binary Coulomb crystal are fully determined by three parameters,  $T/T_s$ ,  $\alpha$ , and  $\beta$ , where  $T_s \equiv \hbar\omega_s$  is the multi-component plasma temperature. If  $\alpha = \beta = 1$ ,  $T_s$  becomes the usual ion plasma temperature of the respective occ,  $T_p \equiv \hbar\omega_p$ .

Using the Holas integration method, we have calculated thermodynamic functions Eq. (12) for the sc2 and h2 lattices in a wide range of  $T/T_s$  and  $\beta$  for dense grids of  $\alpha$  spanning the stability bands of these lattices. The numerical data on the thermodynamic functions are available upon request. Here, we summarize the main features of these results.

Let us recall, that the thermodynamic functions of a Coulomb occ have two asymptotic regimes of high and low (or classic and quantum) temperatures. At high temperatures, where the occupation numbers are big for all phonon modes, the Dulong-Petit law takes place, which states that the heat capacity saturates at  $C_{\text{occ}} = 3N$ , the thermal energy is  $U_{\text{occ}} = 3NT$ , and the free energy is  $F_{\text{occ}} = 3NT[\ln(T_p/T) + u_{\ln}] - 1.5N\hbar\omega_p u_1$ . At low temperatures, only acoustic phonons near the Brillouin zone center are excited and contribute to the thermodynamic quantities. This results in the Debye  $T^3$ -law for the heat capacity and  $T^4$ -law for the energy and free energy.

The Dulong-Petit and Debye laws are also satisfied for binary mixtures (bin). At high temperatures,  $F_{\text{bin}} = 3NT[\ln(T_s/T) + u_{\ln}(\alpha, \beta)] - 1.5N\hbar\omega_s u_1(\alpha, \beta)$ . At low temperatures, the heat capacity behaves as  $C_{\text{bin}} = NH(\alpha, \beta)(T/T_s)^3$ , where  $H(\alpha, \beta)$  is a quantum asymptote coefficient, which depends on  $\alpha$ ,  $\beta$ , and the lattice type. Furthermore,  $F_{\text{bin}} = C_{\text{bin}}T/12$  and  $U_{\text{bin}} = C_{\text{bin}}T/4$ .

In Figs. 11 and 12, we plot the ratios of the three thermodynamic functions of binary mixtures for several  $\alpha$  and  $\beta$  to the same thermodynamic functions of the occ ( $\alpha = \beta = 1$ ) with respective lattice (i.e., bcc for the sc2-mixtures and hcp for the h2-mixtures). The ratios are calculated as functions of  $T/T_s$ , while the thermodynamic functions in the denominator are taken at  $T/T_p = T/T_s$ . Accordingly, to find the value of a thermodynamic function of a binary crystal at  $T/T_s = x_0$ , one has to take the ratio at argument  $x_0$  and multiply by the thermodynamic function of the occ at  $T/T_p = x_0$ . The latter can be taken from Ref. 8 for the bcc crystal and will be published elsewhere<sup>42</sup> for the hcp crystal.

In Fig. 11(a), we consider the thermodynamic functions at  $\alpha = 1$  for several representative values of  $\beta$ , for both types of lattices. One can see that the dependencies are qualitatively very similar for the ratios of different thermodynamic functions. The energy and heat capacity ratios tend to 1 at high temperatures and to a constant, which depends on  $\beta$  but not on the lattice type, at low temperatures. The free energy ratio also tends to the same constant in the quantum limit but at high temperatures, due to the logarithmic character of the asymptotes, its convergence to 1 is much slower. The thermodynamic functions in the quantum regime are higher for mixtures with  $\alpha = 1$  and  $\beta \neq 1$  than for the occ, which can be attributed to softening of acoustic modes near the Brillouin zone center (cf. Figs. 3 and 5). In general, for  $\alpha = 1$ , there is only a slight difference between the lattice types.

The situation is drastically different in Fig. 11(b), where  $\alpha = 1.2$ . In this case, the behavior of the ratios, including their low temperature limits, is very sensitive to the lattice type. Since  $\alpha = 1.2$  is already close to the lattice destruction

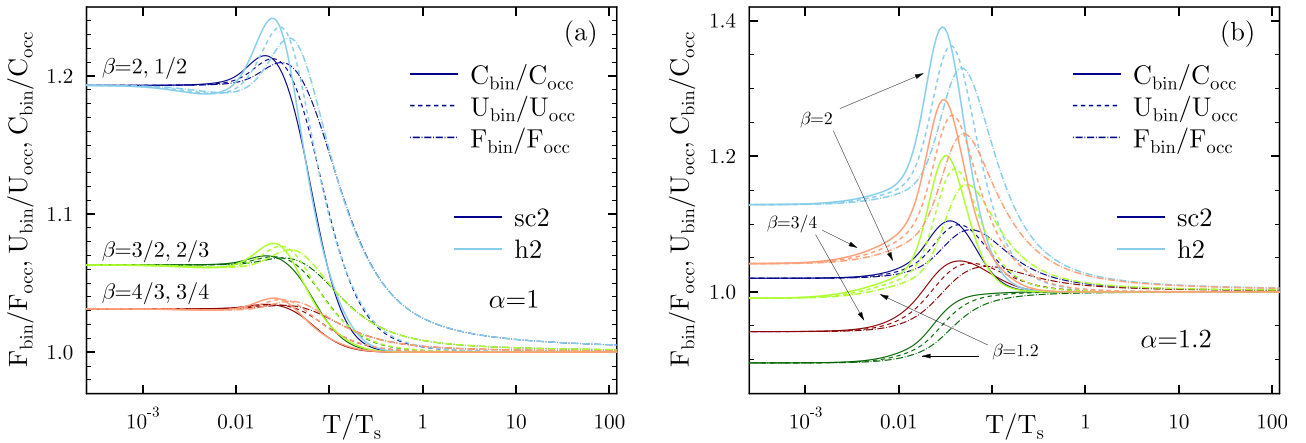


FIG. 11. Ratio of heat capacity, thermal energy and thermal free energy of a binary lattice (sc2 or h2) at different  $\beta$  and  $\alpha = 1$  (a) or  $\alpha = 1.2$  (b) to heat capacity, thermal energy and thermal free energy of the respective occ (bcc or hcp).

for the h2 mixture, one observes a strong increase of the ratios (and thermodynamic functions) at intermediate temperatures. It can be explained by a strong reduction of phonon mode frequencies near the Brillouin zone point H (cf. Fig. 4), as  $\alpha$  approaches 1.25.

The heat capacity ratio at  $\alpha \geq 2$  is plotted in Fig. 12 for the sc2 lattice only. At such  $\alpha$ , the sound speed increases in some directions of the wavevector and decreases in some other (cf. Fig. 2), the net effect being a reduction of the thermodynamic functions of the mixtures in the quantum limit. For some combinations of parameters (most notably  $\alpha = 2$ ,  $\beta = 3$ , and  $\alpha = 3.5$ ,  $\beta = 3.5$ ), an interesting structure with a hump and a trough can be observed at intermediate  $T/T_s$ . Most likely it is associated with a gradually emerging gap between the upper and lower frequencies with increase of  $\beta$  (cf. Fig. 3, where the gap around  $\omega \approx 0.4\omega_s$  is already fully developed at  $\beta = 10$  in the directions shown).

At very high  $\beta$ , due to the wide separation between the upper and lower modes (Sect. IV), the thermodynamic functions of a mixture demonstrate a rather peculiar behavior. There exists a range of temperatures, where the three lower modes are fully excited, while the three upper ones are still exponentially suppressed (Fig. 6). The specific heat becomes equal to 1.5 and stays at this value for a wide range of

intermediate temperatures. When the temperature exceeds  $T_s$ , the specific heat approaches 3. It thus has a pronounced staircase shape. Similar effects take place for the energy and free energy. In Fig. 13 ( $\alpha = 1$ ,  $\beta = 10^5$ ), the dashed line shows the contribution to the specific heat of the three lower modes, while the solid line is the total specific heat of the sc2 lattice.

Based on the numerical data, we have found a convenient fitting formula for the quantum asymptote coefficient

$$H(\alpha, \beta) = H_0 \frac{a_0 + a_1 \alpha + a_2 \alpha^2 + a_3 \alpha^3}{16\sqrt{2}\alpha^{2.5}(1 + b_1 \alpha + b_2 \alpha^2 + b_3 \alpha^3)} \times (1 + \alpha)^{3/2} (1 + \beta)^{3/2} \left(1 + \frac{\alpha}{\beta}\right)^{3/2}, \quad (13)$$

where  $a_i$ ,  $b_i$  are given in Table II. By construction of the fit  $H(1, 1) = H_0$ , where  $H_0 = 2512.0$  and  $2988.2$  for the bcc and hcp crystals, respectively. The dependence of  $H(\alpha, \beta)$  on  $\beta$  is very simple.  $H$  has a minimum at  $\beta = \sqrt{\alpha}$ , and also  $H(\alpha, \beta) = H(\alpha, \alpha/\beta)$ . At  $\alpha = 1$ , this reflects the fact that mixtures with  $\beta = \beta_0$  and  $\beta = 1/\beta_0$  are identical (see Fig. 11(a)). The validity of this equality at  $\alpha = 2$  is seen in Fig. 12, where the curves with  $\beta = \beta_0$  and  $\beta = 2/\beta_0$  merge at low temperatures.

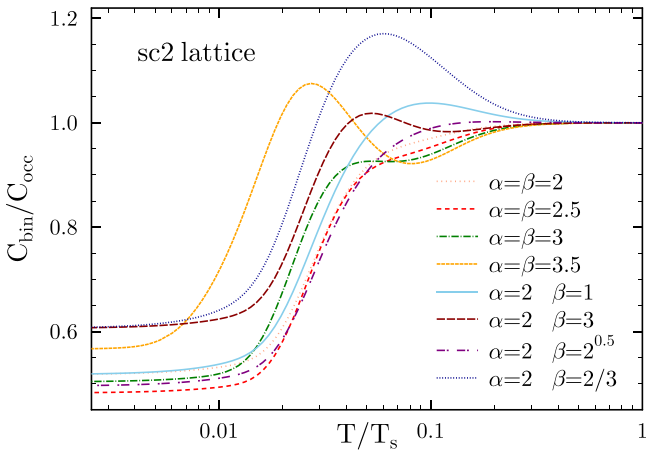


FIG. 12. Ratio of heat capacity of the sc2 lattice at different  $\alpha$  and  $\beta$  to heat capacity of the bcc lattice.

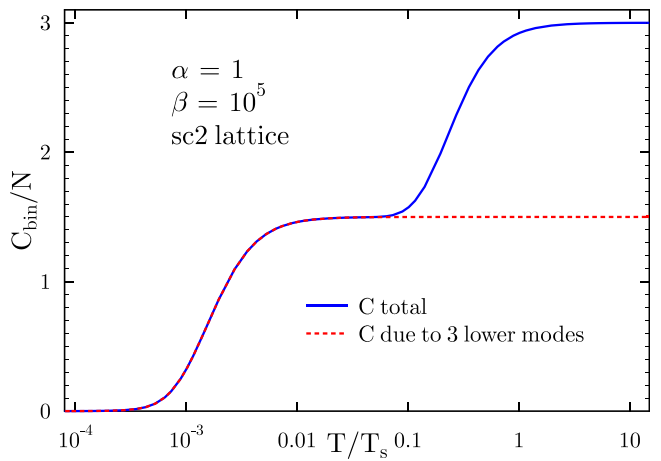


FIG. 13. Heat capacity for the sc2 lattice at  $M_2 \gg M_1$  and  $\alpha = 1$ .

TABLE II. Fitting parameters  $a_i$  and  $b_i$  for the sc2 and h2 lattices (accuracy exceeds 0.2% and 0.05%, respectively).

	$i$	0	1	2	3
sc2	$a_i$	0.1236	-0.22915	0.2297	0.03881
	$b_i$		-2.024	1.354	-0.1671
h2	$a_i$	0.0610816	0.236187	-0.0393898	-0.0357678
	$b_i$		-1.78839	1.41519	-0.404688

Finally, it is worthwhile to compare the thermodynamic functions of a one-to-one Coulomb crystal mixture calculated using the linear mixing theory with the exact results obtained from the phonon spectrum. Using the heat capacity as an example and following Ref. 18, we can write  $C_{\text{lm}} = N_1 C_1(Z_1, M_1) + N_2 C_2(Z_2, M_2)$ , where  $C_i(Z_i, M_i)$  is the specific heat of the occ at the same temperature and electron number density as in the mixture. Our calculations show noticeable deviation of the lm predictions from the exact results at intermediate and low temperatures for crystals with significant difference between ions (Fig. 14). For example, for  $\alpha=2$  and  $\beta=1$ , the specific heat calculated by the lm rule is 2.4 times greater than the actual one at low temperatures. For the carbon-oxygen mixture ( $^{12}\text{C}+^{16}\text{O}$ ),  $C_{\text{lm}}/C_{\text{bin}}$  varies from 1 at  $T/T_s \sim 1$  to 1.268 at  $T \ll T_s$ . In Fig. 14, only for the  $^{62}\text{Ni}+^{78}\text{Ni}$  and  $^{56}\text{Fe}+^{62}\text{Ni}$  mixtures, the difference between  $C_{\text{lm}}$  and  $C_{\text{bin}}$  at low temperatures is small and does not exceed a few percent. For these two mixtures, the right-hand y-axis should be used. Similar conclusions also hold true for the thermal energy and thermal free energy.

## VII. CONCLUSIONS

We have studied physical properties of ordered Coulomb crystal mixtures from the first principles in the harmonic lattice model. We have derived rapidly converging practical expressions for the electrostatic energy and the dynamic matrix of an arbitrary multi-component Coulomb crystal. The general expressions have been applied to binary Coulomb crystals with equal number of ions of two different types with sc2 and h2 lattices, and these systems have been

analyzed in considerable detail (the sc2 and h2 lattices turn into the bcc and hcp lattices if all ions are identical).

We have confirmed our earlier findings that the sc2 and h2 lattices are stable if the ratio of ion charges  $\alpha$  in the binary crystal is below 3.60 and 1.25, respectively, regardless of the ion mass ratio  $\beta$  (by definition  $\alpha \geq 1$ ). We have also compared the exact binary crystal electrostatic energy with that obtained from the linear mixing theory. The relative inaccuracy of the latter for the electrostatic energy is shown to be not worse than a few parts per thousand.

The dynamic matrix allows one to determine the phonon spectrum of a crystal. Phonon spectrum moments and thermodynamic functions have been calculated by numerical integration over the first Brillouin zone for a wide range of temperatures,  $\alpha$ , and  $\beta$ . For all mixtures, the Dulong-Petit and Debye laws are satisfied. The dependence of the Debye-law coefficient on  $\alpha$  and  $\beta$  have been approximated by a convenient analytic formula with good accuracy for both lattices. We have also investigated the phonon properties for binary crystals with very different ion masses ( $\beta \gg 1$ ). In this limit, a gap develops in the crystal spectrum, which separates the low-frequency ( $\sim \omega_s/\sqrt{\beta}$ ) modes, corresponding to a joint motion of both types of ions, from the high-frequency ( $\sim \omega_s$ ) modes, describing the oscillations of the lighter ions with respect to the heavier ones. As a result, the spectrum moments have very simple asymptotic behavior. Also, the temperature dependence of the crystal thermodynamic functions assumes a pronounced staircase shape, because the low-frequency modes saturate at temperatures, where the high-frequency modes are still exponentially suppressed.

Finally, we have checked the accuracy of the linear mixing predictions for the phonon thermodynamic functions against our results based on the actual phonon spectra of binary mixtures. It turned out that the linear mixing theory does a rather poor job being off by tens to hundreds per cent at intermediate and low temperatures, especially, for crystals with significantly different ions.

## ACKNOWLEDGMENTS

The work of A.A.K. was partially supported by Russian Foundation for Basic Research (Grant No. 14-02-00868-a).

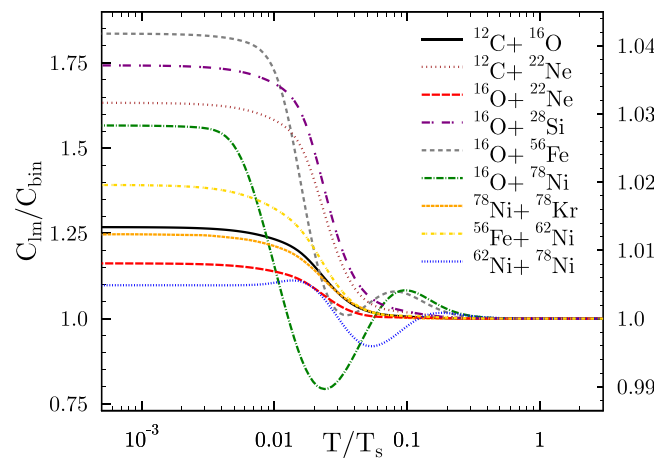


FIG. 14. Ratio of the linear mixing theory specific heat to the exact phonon specific heat of the mixture. The right-hand y-axis should be used for  $^{62}\text{Ni}+^{78}\text{Ni}$  and  $^{56}\text{Fe}+^{62}\text{Ni}$  mixtures.

- <sup>1</sup>P. Haensel, A. Y. Potekhin, and D. G. Yakovlev, *Neutron Stars 1: Equation of State and Structure* (Springer, New York, 2007).
- <sup>2</sup>L. Segretain, G. Chabrier, M. Hernanz, E. Garcia-Berro, J. Isern, and R. Mochkovitch, *Astrophys. J.* **434**, 641 (1994).
- <sup>3</sup>D. E. Winget, S. O. Kepler, F. Campos, M. H. Montgomery, L. Girardi, P. Bergeron, and K. Williams, *Astrophys. J.* **693**, L6 (2009).
- <sup>4</sup>S. L. Shapiro and S. A. Teukolsky, *Black Holes, White Dwarfs, and Neutron Stars* (Wiley-Interscience, New York, 1983).
- <sup>5</sup>W. J. Carr, Jr., *Phys. Rev.* **122**, 1437 (1961).
- <sup>6</sup>E. L. Pollock and J. P. Hansen, *Phys. Rev. A* **8**, 3110 (1973).
- <sup>7</sup>G. Chabrier, *Astrophys. J.* **414**, 695 (1993).
- <sup>8</sup>D. A. Baiko, A. Y. Potekhin, and D. G. Yakovlev, *Phys. Rev. E* **64**, 057402 (2001).
- <sup>9</sup>A. Y. Potekhin and G. Chabrier, *Contrib. Plasma Phys.* **50**, 82 (2010).
- <sup>10</sup>D. A. Baiko, *Phys. Rev. E* **80**, 046405 (2009).
- <sup>11</sup>D. A. Baiko and D. G. Yakovlev, *MNRAS* **433**, 2018 (2013).
- <sup>12</sup>A. Y. Potekhin and G. Chabrier, *Phys. Rev. E* **62**, 8554 (2000).
- <sup>13</sup>D. A. Baiko, *Phys. Rev. E* **66**, 056405 (2002).
- <sup>14</sup>M. Akbari-Moghanjoughi, *Phys. Plasmas* **20**, 042706 (2013).

- <sup>15</sup>R. C. Albers and J. E. Gubernatis, *Phys. Rev. B* **33**, 5180 (1986).
- <sup>16</sup>D. H. E. Dubin, *Phys. Rev. A* **42**, 4972 (1990).
- <sup>17</sup>A. Y. Potekhin, G. Chabrier, and F. J. Rogers, *Phys. Rev. E* **79**, 016411 (2009).
- <sup>18</sup>G. Chabrier and N. W. Ashcroft, *Phys. Rev. A* **42**, 2284 (1990).
- <sup>19</sup>Z. Medin and A. Cumming, *Phys. Rev. E* **81**, 036107 (2010).
- <sup>20</sup>C. J. Horowitz and D. K. Berry, *Phys. Rev. C* **79**, 065803 (2009).
- <sup>21</sup>A. S. Schneider, J. Hughto, C. J. Horowitz, and D. K. Berry, *Phys. Rev. E* **85**, 066405 (2012).
- <sup>22</sup>J. Hughto, C. J. Horowitz, A. S. Schneider, Z. Medin, A. Cumming, and D. K. Berry, *Phys. Rev. E* **86**, 066413 (2012).
- <sup>23</sup>S. Ichimaru, H. Iyetomi, and S. Ogata, *Astrophys. J.* **334**, L17 (1988).
- <sup>24</sup>G. S. Stringfellow, H. E. DeWitt, and W. L. Slattery, *Phys. Rev. A* **41**, 1105 (1990).
- <sup>25</sup>H. E. DeWitt, W. Slattery, and G. Chabrier, *Physica B* **228**, 21 (1996).
- <sup>26</sup>H. E. DeWitt and W. Slattery, *Contrib. Plasma Phys.* **43**, 279 (2003).
- <sup>27</sup>J. P. Hansen, G. M. Torrie, and P. Vieillefosse, *Phys. Rev. A* **16**, 2153 (1977).
- <sup>28</sup>Y. Rosenfeld, *Phys. Rev. E* **52**, 3292 (1995); **54**, 2827 (1996).
- <sup>29</sup>S. Ogata, H. Iyetomi, S. Ichimaru, and H. M. Van Horn, *Phys. Rev. E* **48**, 1344 (1993).
- <sup>30</sup>A. A. Kozhberov and D. A. Baiko, *Contrib. Plasma Phys.* **52**, 153 (2012).
- <sup>31</sup>P. P. Ewald, *Ann. Phys.* **359**, 519 (1917); **369**, 253 (1921).
- <sup>32</sup>K. Fuchs, *Proc. R. Soc. London, Ser. A* **151**, 585 (1935); **153**, 622 (1936); **157**, 444 (1936).
- <sup>33</sup>A. A. Kozhberov and D. A. Baiko, *Contrib. Plasma Phys.* **54**, 859 (2014).
- <sup>34</sup>T. Nagai and H. Fukuyama, *J. Phys. Soc. Jpn.* **51**, 3431 (1982); **52**, 44 (1983).
- <sup>35</sup>W. Setyawana and S. Curtaroloa, *Comput. Mater. Sci.* **49**, 299 (2010).
- <sup>36</sup>M. Born, *Proc. Cambr. Philos. Soc.* **36**, 160 (1940).
- <sup>37</sup>M. Born, *Proc. Cambr. Philos. Soc.* **38**, 82 (1942).
- <sup>38</sup>G. J. Kalman, Z. Donko, P. Hartmann, and K. I. Golden, *Europhys. Lett.* **107**, 35001 (2014).
- <sup>39</sup>A. Holas, *J. Comput. Phys.* **23**, 150 (1977).
- <sup>40</sup>R. C. Albers and J. E. Gubernatis, LASL Report No. LA-8674-MS, 1981.
- <sup>41</sup>A. A. Kozhberov, Ph.D. thesis (Ioffe Institute, in prep.).
- <sup>42</sup>A. A. Kozhberov and D. A. Baiko, “Thermodynamic functions of the hcp Coulomb crystal Lattice,” *Astrophys. Space Sci.* (to be published).